The Astrophysical Journal, 870:106 (7pp), 2019 January 10 https://doi.org/10.3847/1538-4357/aaef77
© 2019. The American Astronomical Society.
OPEN ACCESS

The Fluid-like and Kinetic Behavior of Kinetic Alfvén Turbulence in Space Plasma

Honghong Wu[1,2], Daniel Verscharen[2,3], Robert T. Wicks[2,4], Christopher H. K. Chen[5], Jiansen He[1], and Georgios Nicolaou[2]

[1] School of Earth and Space Sciences, Peking University, Beijing, People's Republic of China
[2] Mullard Space Science Laboratory, University College London, Surrey, UK
[3] Space Science Center, University of New Hampshire, Durham NH, USA
[4] Institute for Risk and Disaster Reduction, University College London, London, UK
[5] School of Physics and Astronomy, Queen Mary University of London, London, UK

Received 2018 August 29; revised 2018 November 6; accepted 2018 November 6; published 2019 January 14

Abstract

Kinetic Alfvén waves (KAWs) are the short-wavelength extension of the magnetohydrodynamics Alfvén-wave branch in the case of highly oblique propagation with respect to the background magnetic field. Observations of space plasma show that small-scale turbulence is mainly KAW-like. We apply two theoretical approaches, a collisional two-fluid theory and a collisionless linear kinetic theory, to obtain predictions for the KAW polarizations depending on β_p (the ratio of the proton thermal pressure to the magnetic pressure) at the ion gyroscale in terms of fluctuations in density, bulk velocity, and pressure. We perform a wavelet analysis of *Magnetospheric Multiscale* magnetosheath measurements and compare the observations with both theories. We find that the two-fluid theory predicts the observations better than the kinetic theory, suggesting that the small-scale KAW-like fluctuations exhibit a fluid-like behavior in the magnetosheath although the plasma is weakly collisional. We also present predictions for the KAW polarizations in the inner heliosphere that are testable with *Parker Solar Probe* and *Solar Orbiter*.

Key words: magnetohydrodynamics (MHD) – plasmas – solar–terrestrial relations – turbulence – waves

1. Introduction

Standard single-fluid magnetohydrodynamics (MHD) contains four linear modes in a collisional plasma: the Alfvén wave, the fast-magnetosonic wave, the slow-magnetosonic wave, and the entropy mode. The polarization and dispersion relations identify their counterparts in the collisionless kinetic theory (Stix 1992; Gary 1993). Due to the collisionless nature of the solar wind, kinetic models have been expected to describe these fluctuations more accurately than MHD. However, Verscharen et al. (2017) compare theoretical predictions for wave polarization properties from both the MHD theory and the kinetic theory with observations of compressive fluctuations in the solar wind and find that the predictions from linear MHD agree better with the observations than the predictions from the kinetic theory for slow modes at large scales. The comparison between the fluid-like and the kinetic behavior of collisionless plasmas is of great importance for our fundamental understanding of plasma turbulence. In this context, we define a fluid-like mode as a plasma mode that follows the predictions from fluid equations with adiabatic and isotropic pressure closure.

The magnetic fluctuations in the inertial range of solar-wind turbulence exhibit Alfvénic correlations (Belcher & Davis 1971) and a scale-dependent anisotropy with $k_\perp \gg k_\parallel$ (Horbury et al. 2008; Wicks et al. 2010; Chen et al. 2011, 2012; He et al. 2013; Yan et al. 2016), where $k_\perp$ is the perpendicular wavenumber and $k_\parallel$ is the parallel wavenumber with respect to the background magnetic field. Kinetic Alfvén waves (KAWs) are the short-wavelength extension of the Alfvén-wave branch in the case of highly oblique propagation with respect to the background magnetic field. Therefore, it is thought that the cascade continues into the KAW-like regime for $k_\perp \rho_p \gtrsim 1$, where $\rho_p = v_{th}/\omega_{cp}$ is the ion gyroscale, v_{th} is the perpendicular thermal speed, $\omega_{cp} = q_p B_0/m_p c$ is the proton gyrofrequency, q_p is the proton electric charge, m_p is the proton mass, B_0 is the magnitude of the background magnetic field, and c is the speed of light. A growing body of evidence corroborates the presence of kinetic Alfvén turbulence in the solar wind (Chandran et al. 2009; Chen et al. 2010, 2013; Sahraoui et al. 2010; He et al. 2011; Salem et al. 2012). Likewise, observations of small-scale fluctuations in the magnetosheath also suggest the presence of KAW-like turbulence (Chen & Boldyrev 2017; Breuillard et al. 2018). We extend the study of Verscharen et al. (2017) to examine KAW-like fluctuations at small scales. In Section 2, we present predictions for fluctuations in the first three velocity moments associated with KAWs from both the collisional two-fluid theory and the collisionless linear kinetic theory. In Section 3, we describe our analysis of *Magnetospheric Multiscale* (*MMS*) magnetosheath measurements. We compare observations with our predictions in Section 4. In Section 5, we discuss our results and present our conclusions. We present predictions for solar-wind measurements with *Parker Solar Probe* and *Solar Orbiter* in the Appendix.

2. Theory

We take the background magnetic field to be $\boldsymbol{B}_0 = (0, 0, B_0)$, the electric field to be $\boldsymbol{E} = \delta\boldsymbol{E}$ ($\delta\boldsymbol{E}$ is the fluctuating electric field), and the wave vector to be $\boldsymbol{k} = (k_\perp, 0, k_\parallel)$. In our coordinate system, the z-direction is parallel to $\boldsymbol{B}_0$, and $\boldsymbol{k}$ lies in the x–z plane. We define the dimensionless quantities ξ_s, $\chi_{\parallel s}$, $\chi_{\perp s}$, and ψ_s as the normalized amplitudes of the fluctuations in

Original content from this work may be used under the terms of the Creative Commons Attribution 3.0 licence. Any further distribution of this work must maintain attribution to the author(s) and the title of the work, journal citation and DOI.

the first three velocity moments of species s through

$$\frac{\delta n_s}{n_{0s}} = \xi_s \frac{\delta B_y}{B_0}, \tag{1}$$

$$\frac{\delta v_{\parallel s}}{v_A} = \chi_{\parallel s} \frac{\delta B_y}{B_0}, \tag{2}$$

$$\frac{\delta v_{ys}}{v_A} = \chi_{\perp s} \frac{\delta B_y}{B_0}, \tag{3}$$

and

$$\frac{\delta P_s}{P_{B0}} = \psi_s \frac{\delta B_y}{B_0}, \tag{4}$$

where $P_{B0} = B_0^2/8\pi$; n_{0s} is the average density of species s, δn_s, $\delta v_{\parallel s}$, δv_{ys}, δP_s, and δB_y are the amplitudes of fluctuations in the number density, the bulk velocity component parallel to $\boldsymbol{B}_0$, the bulk velocity component in the y-direction, the thermal pressure, and the magnetic-field component in the y-direction, respectively. We note that ξ_s, $\chi_{\parallel s}$, $\chi_{\perp s}$ and ψ_s are complex and include information about the phases between the fluctuating quantities. We consider a plasma consisting of protons ($s = \mathrm{p}$) and electrons ($s = \mathrm{e}$) only and neglect all of the effects of temperature anisotropies.

2.1. Two-fluid Model

The two-fluid dispersion relation follows from linearizing the continuity, momentum, and energy equations and Maxwell's equations. We rewrite the two-fluid solutions of Hollweg (1999) for the dispersion relation of KAWs using our coordinate system. The KAW dispersion relation is then given by

$$\omega^2 = \frac{k_\parallel^2 v_A^2}{2\left(1 + G + k_\perp^2 d_p^2 \frac{m_e}{m_p}\right)} \left\{ 1 + 2G + G k_\perp^2 d_p^2 + \left[\left(1 + G k_\perp^2 d_p^2\right)^2 + 4G k_\perp^2 d_p^2 \left(G - \frac{m_e}{m_p} \right) \right]^{1/2} \right\}, \tag{5}$$

where $v_A = B_0/\sqrt{4\pi n_{0p} m_p}$ is the Alfvén speed, $d_p = v_A/\omega_{cp}$ is the ion inertial length, $G = (\gamma_p \beta_p + \gamma_e \beta_e)/2$,

$$\beta_s = \frac{8\pi n_{0s} \kappa_B T_s}{B_0^2}, \tag{6}$$

γ_s is the specific heat ratio of species s, m_e is the electron mass, T_s is the parallel temperature of species s, and κ_B is Boltzmann constant.

We calculate the quantities ξ_p, $\chi_{\parallel p}$, $\chi_{\perp p}$, and ψ_p as

$$\xi_p = \frac{2i(\omega^2 - k_\parallel^2 v_A^2)}{k_\perp d_p \left[\omega^2 (2m_e/m_p - \gamma_p \beta_p) - \gamma_e \beta_e k_\parallel^2 v_A^2 \right]} \times \frac{\omega}{v_A \left(k_\parallel - k_\perp \frac{\delta E_z}{\delta E_x} \right)}, \tag{7}$$

$$\chi_{\parallel p} = \left[\frac{i\omega_{cp}}{\omega} + \frac{i\gamma_p \beta_p \omega_{cp} k_\parallel^2 v_A^2}{\omega(\gamma_e \beta_e k_\parallel^2 v_A^2 - 2\omega^2 m_e/m_p)} \right] \frac{\delta E_z}{\delta E_x} \times \frac{\omega}{v_A \left(k_\parallel - k_\perp \frac{\delta E_z}{\delta E_x} \right)}, \tag{8}$$

$$\chi_{\perp p} = \left[-1 - \frac{i\omega \frac{\delta E_y}{\delta E_x}}{\omega_{cp}} - \frac{\gamma_p \beta_p k_\perp k_\parallel v_A^2 \frac{\delta E_z}{\delta E_x}}{\gamma_e \beta_e k_\parallel^2 v_A^2 - 2\omega^2 m_e/m_p} \right] \times \frac{\omega}{v_A \left(k_\parallel - k_\perp \frac{\delta E_z}{\delta E_x} \right)}, \tag{9}$$

and

$$\psi_p = \gamma_p \beta_p \xi_p, \tag{10}$$

where

$$\frac{\delta E_y}{\delta E_x} = \frac{-i\omega\omega_{cp}(\gamma_p \beta_p + \gamma_e \beta_e)}{\left[\omega^2 (\gamma_p \beta_p - 2m_e/m_p) + \gamma_e \beta_e k_\parallel^2 v_A^2 \right]} \times \frac{\omega^2 - k_\parallel^2 v_A^2}{\omega^2 - k_\parallel^2 v_A^2 - k_\perp^2 v_A^2} \tag{11}$$

and

$$\frac{\delta E_z}{\delta E_x} = \frac{(\omega^2 - k_\parallel^2 v_A^2)(\gamma_e \beta_e k_\parallel^2 v_A^2 - 2\omega^2 m_e/m_p)}{k_\parallel k_\perp v_A^2 \left[\omega^2 (2m_e/m_p - \gamma_p \beta_p) - \gamma_e \beta_e k_\parallel^2 v_A^2 \right]}. \tag{12}$$

2.2. Kinetic Theory

The linear kinetic hot-plasma dispersion relation follows from linearizing the Vlasov equation and Maxwell's equations (see, e.g., Stix 1992, Chapter 10). We assume that both protons and electrons have isotropic Maxwellian background distribution functions. The dispersion relation is then given by the nontrivial solutions to the wave equation,

$$\frac{\boldsymbol{k}c}{\omega} \times \left(\frac{\boldsymbol{k}c}{\omega} \times \delta \boldsymbol{E} \right) + \epsilon \delta \boldsymbol{E} \equiv \boldsymbol{D} \delta \boldsymbol{E} = 0, \tag{13}$$

where ϵ is the dielectric tensor. We note that ω is complex. The electric current density fulfills

$$\boldsymbol{j} = \sum_s \boldsymbol{j}_s = -\frac{i\omega}{4\pi} \sum_s \boldsymbol{\sigma}_s \cdot \delta \boldsymbol{E}, \tag{14}$$

where $\boldsymbol{j}_s$ is the current density contribution from species s, $\boldsymbol{\sigma}_s$ is the susceptibility tensor of species s, and $\epsilon = 1 + \sum_s \boldsymbol{\sigma}_s$.

The linearized continuity equation connects the fluctuations of the density with the fluctuations of the current density,

$$-\omega q_s n_{0s} \delta n_s + \boldsymbol{k} \cdot \boldsymbol{j}_s = 0. \tag{15}$$

Therefore, we find

$$\xi_s = \frac{-iB_0}{4\pi n_{0s}^2 q_s} \boldsymbol{k} \cdot \left(\boldsymbol{\sigma}_s \cdot \frac{\delta \boldsymbol{E}}{\delta B_y} \right). \tag{16}$$

The electric current density also fulfills

$$\boldsymbol{j} = \sum_s \boldsymbol{j}_s = \sum_s q_s \int \boldsymbol{v}\, \delta f_s\, d^3\boldsymbol{v}, \tag{17}$$

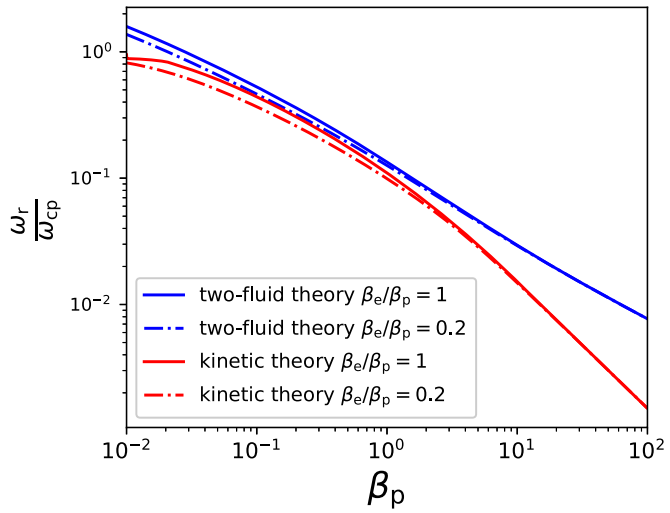

Figure 1. Real part of the frequency of KAWs with $k_\perp \rho_p = 2$ as a function of β_p from the two-fluid theory (blue) and kinetic theory (red). We use $\theta_{kB} = 88°$, $\gamma_p = 5/3$, and $\gamma_e = 1$, where θ_{kB} is the angle between the direction of wave propagation and the background magnetic field. The solid and dashed–dotted lines represent $\beta_e/\beta_p = 1$ and $\beta_e/\beta_p = 0.2$ respectively. The two-fluid theory and kinetic theory agree quantitively. The value of β_e/β_p affects the predictions.

leading to

$$\chi_{\parallel s} = \frac{-i\omega B_0}{4\pi n_{0s} q_s v_A}\left(\boldsymbol{\sigma}_s \cdot \frac{\delta \boldsymbol{E}}{\delta B_y}\right)_z \tag{18}$$

and

$$\chi_{\perp s} = \frac{-i\omega B_0}{4\pi n_{0s} q_s v_A}\left(\boldsymbol{\sigma}_s \cdot \frac{\delta \boldsymbol{E}}{\delta B_y}\right)_y. \tag{19}$$

The fluctuations in pressure follow from the second moment of the fluctuations in the distribution δf_s,

$$\psi_{\parallel s} = \frac{n_{0s} m_p B_0}{P_{B0}\delta B_y}\int v_\parallel^2 \delta f_s \, d^3v \tag{20}$$

and

$$\psi_{\perp s} = \frac{n_{0s} m_p B_0}{2P_{B0}\,\delta B_y}\int v_\perp^2 \delta f_s \, d^3v. \tag{21}$$

We define fluctuations in the total pressure as

$$\psi_s = \frac{1}{3}\psi_{\parallel s} + \frac{2}{3}\psi_{\perp s}. \tag{22}$$

The New Hampshire Dispersion relation Solver (NHDS) code (Verscharen & Chandran 2018) solves the hot-plasma dispersion relation of the linearized Vlasov–Maxwell system and determines the polarization properties numerically. Figure 1 shows NHDS solutions for ω_r (the real part of the frequency) of KAWs with $k_\perp \rho_p = 2$ as functions of β_p for $\beta_e/\beta_p = 1$ and $\beta_e/\beta_p = 0.2$. In addition, we show KAW solutions from our two-fluid theory with the same parameters and $\gamma_p = 5/3$ and $\gamma_e = 1$. The dispersion relations agree quantitatively well, especially for $\beta_p \lesssim 1$.

3. Data Analysis

We analyze data from the four *MMS* spacecraft (Burch et al. 2016). In burst mode, the Fast Plasma Investigation (FPI) instrument provides proton moments every 150 ms and electron moments every 30 ms (Pollock et al. 2016). The fluxgate magnetometer (FGM) measures the magnetic field with a resolution of <1 ms. We select intervals in the magnetosheath from 2015 October 1 to 2018 February 28 based on the quicklook archive of *MMS*. We split every interval into 10 s intervals with an overlap of 5 s. We remove data intervals in which $\max[|n_p - n_e|/n_p] > 0.1$.

Magnetosheath plasma exhibits fluctuations not related to pure turbulence, e.g., instability-generated waves (such as mirror modes, ion-cyclotron waves, and whistler waves) and various other non-turbulent structures (see, e.g., Lucek et al. 2005). In order to investigate the turbulence itself, we eliminate intervals with $\max(\beta_p) - \min(\beta_p) > \beta_{0p}$ and $\max(n_p) - \min(n_p) > 0.2\, n_{0p}$, where the subscript 0 represents the average over the 10 s interval. We also remove data intervals in which $v_{0p} < v_A$, where v_{0p} is the average ion bulk velocity so that Taylor's hypothesis applies (Taylor 1938; Klein et al. 2014). For each interval, we calculate β_{0p} and β_{0e}. We find that the average ratio $\beta_{0e}/\beta_{0p} \approx 0.21$ with a standard deviation of 0.09 and, therefore, set $\beta_e/\beta_p = 0.2$ in our study. The averaged normalized amplitude of the fluctuations in $\delta B_\perp$ is $\delta B_\perp/B_0 = 0.05$ with a standard deviation of 0.04, and the averaged normalized amplitude of the fluctuations in magnetic-field amplitude is $\delta|\boldsymbol{B}|/B_0 = 0.07$ with a standard deviation of 0.05. The Columb collision frequency ν_{ei} is 7×10^{-5} Hz under the conditions in our data set: $n_e \approx 25\,\mathrm{cm}^{-3}$, $T_e \approx 50$ eV, corresponding to a mean free path of $\lambda \approx 2 \times 10^7$ km for $v_{0p} \approx 150\,\mathrm{km\,s}^{-1}$. Since $\lambda/d_p \approx 1500$, we consider the plasma to be collisionless.

In order to study the scale-dependent behavior of the fluctuations, we apply a continuous wavelet transform based on the Morlet wavelet (Torrence & Compo 1998) to n_p, all components of $\boldsymbol{v}_p$ and $\boldsymbol{B}$, and to every element of the proton pressure tensor $\boldsymbol{P}_p$. We obtain the fluctuation amplitudes δn_p, $\delta \boldsymbol{v}_p$, $\delta \boldsymbol{B}$, and $\delta \boldsymbol{P}_p$ from the absolute wavelet coefficients as functions of both scale ℓ (16 logarithmically spaced scales) and time t. We calculate the local magnetic field and the local velocity at wavelet scale ℓ and time t_n by weighting the time series with a Gaussian curve centered at time t_n (Horbury et al. 2008; Podesta 2009) as

$$\boldsymbol{C}_n = \frac{\sum_{m=0}^{N-1} \boldsymbol{C}_m \exp\left[-\frac{(t_n - t_m)^2}{2\ell^2}\right]}{\sum_{m=0}^{N-1} \exp\left[-\frac{(t_n - t_m)^2}{2\ell^2}\right]}, \tag{23}$$

where N is the number of data points and $\boldsymbol{C}$ is either $\boldsymbol{B}$ or $\boldsymbol{v}$. In this way, we obtain the local mean magnetic field $\boldsymbol{B}_0$, the local mean velocity $\boldsymbol{v}_{0p}$, the angle between local mean velocity and local mean magnetic field θ_{vB}, as well as β_p and ρ_p as functions of ℓ and t_n.

We find that $\delta B_y \gg \delta B_x$ for KAWs in both the two-fluid theory and the kinetic theory. Therefore, we use $\delta B_\perp \approx \delta B_y$ and exploit the azimuthal symmetry of a gyrotropic distribution of the fluctuating energy. We calculate the parallel and perpendicular fluctuations by

$$\delta \boldsymbol{C}_\parallel = \frac{|\delta \boldsymbol{C} \cdot \boldsymbol{B}_0|}{|\boldsymbol{B}_0|} \tag{24}$$

and

$$\delta \boldsymbol{C}_\perp = \frac{|\boldsymbol{B}_0 \times (\delta \boldsymbol{C} \times \boldsymbol{B}_0)|}{|\boldsymbol{B}_0|^2}, \tag{25}$$

where $\delta \boldsymbol{C}$ is either $\delta \boldsymbol{v}_p$ or $\delta \boldsymbol{B}$.

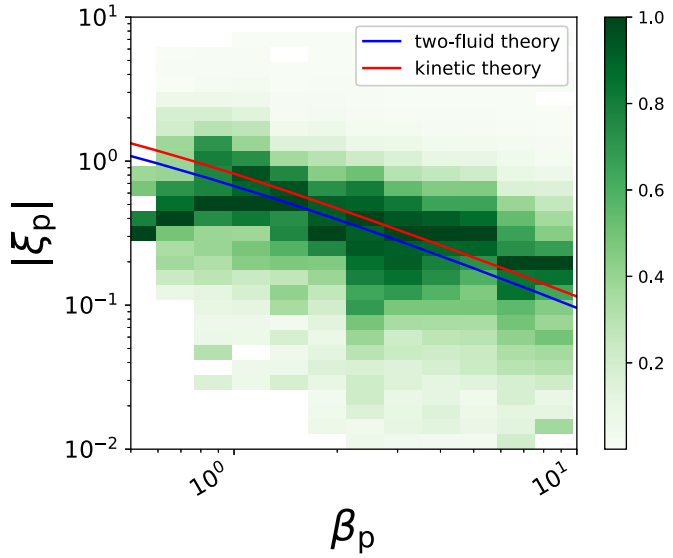

Figure 2. Ratio of proton density fluctuations and perpendicular magnetic-field fluctuations, ξ_p, as a function of β_p at $k_\perp \rho_i \approx 2$. The lines show our theoretical results and the color coded bins show the logarithmically scaled, column-normalized data distribution in the ξ_p–β_p plane. The theoretical predictions from the two-fluid theory and kinetic theory are similar, and the observations agree with both models.

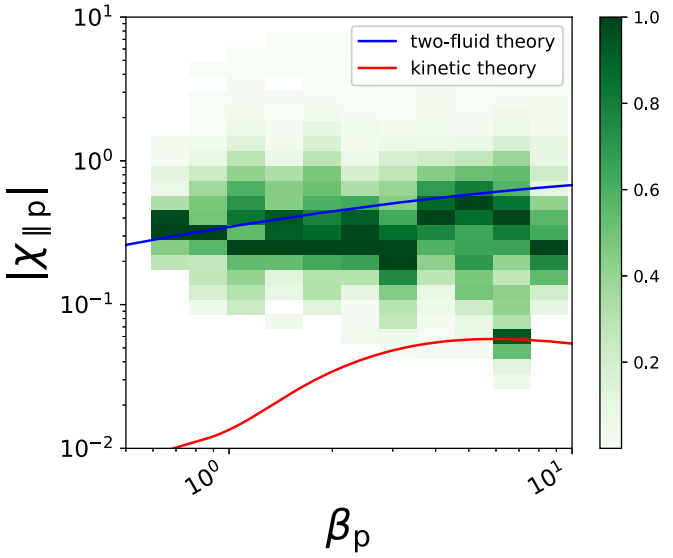

Figure 3. Ratio of parallel proton velocity fluctuations and perpendicular magnetic-field fluctuations, $\chi_{\parallel p}$, as a function of β_p at $k_\perp \rho_p \approx 2$ with the same panel and line styles as Figure 2. The theoretical predictions for $\chi_{\parallel p}$ from the two-fluid theory are significantly greater than those from the kinetic theory, and the observations agree better with the two-fluid theory than with the kinetic theory.

We obtain the transformation matrix α_{ij} from the Geocentric Solar Ecliptic coordinate system to the field-aligned coordinate system with respect to $\boldsymbol{B}_0$ and then transform the tensor of pressure fluctuations δP_{pij} to the field-aligned coordinate system by

$$\delta P'_{pij} = \alpha_{ki}\, \delta P_{pkm}\, \alpha_{mj}. \tag{26}$$

The total proton thermal pressure is given by

$$\delta P_p = \frac{1}{3}\left(\delta P'_{p11} + \delta P'_{p22} + \delta P'_{p33}\right). \tag{27}$$

For each scale ℓ and time t_n, we determine $k_\perp$ as

$$k_\perp \rho_p = \frac{2\pi \rho_p}{\ell\, v_{0p} \sin(\theta_{vB})}, \tag{28}$$

and retain only coefficients with $1.8 \leqslant k_\perp \rho_p \leqslant 2.2$ and $60^\circ < \theta_{vB} < 120^\circ$.

In order to remove noise in our measurements, we only retain coefficients when $\delta v_{\parallel p} > 1.0\,\mathrm{km\,s^{-1}}$ and $\delta v_{\perp p} > 1.0\,\mathrm{km\,s^{-1}}$. We then construct a set of 600 bins in logarithmic space of β_p and the value of the coefficients, count the number of occurrences in each bin, normalize each bin by its width, and then column-normalize the histogram.

4. Results

Figure 2 shows the zeroth proton velocity moment ξ_p depending on β_p in the two-fluid and kinetic theory and our *MMS* observations for $k_\perp \rho_p = 2$. The two-fluid theory and kinetic theory predict similar values for ξ_p under these parameters. Therefore, the observations of the zeroth moment do not favor the applicability of either theory unambiguously. However, the data agree well with the theoretical predictions as well as previous observations (Chen et al. 2013; Chen & Boldyrev 2017) and thus support the applicability of our data analysis technique and the model comparisons.

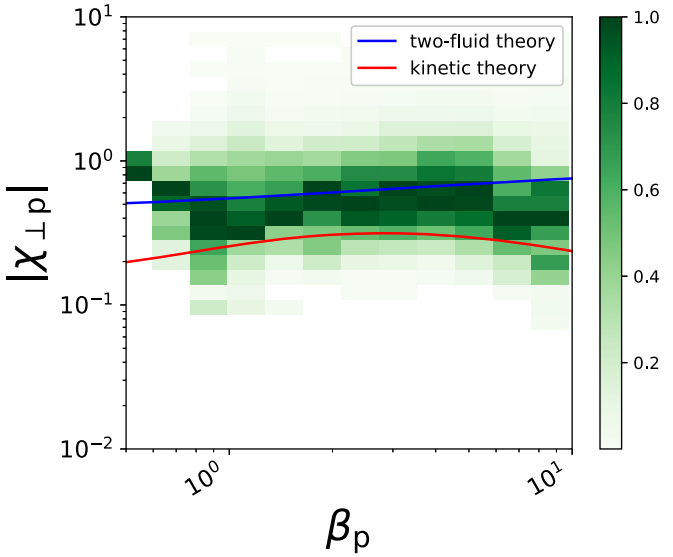

Figure 4. Ratio of perpendicular proton velocity fluctuations and perpendicular magnetic-field fluctuations, $\chi_{\perp p}$, as a function of β_p at $k_\perp \rho_p \approx 2$ with the same panel and line styles as Figure 2. The theoretical predictions for $\chi_{\perp p}$ from the two-fluid theory are greater than the predictions from the kinetic theory, and the observations agree with both the two-fluid theory and kinetic theory with a small bias toward the two-fluid theory.

Figure 3 shows the first parallel proton velocity moment $\chi_{\parallel p}$ depending on β_p in both theories and our *MMS* observations. For all shown values of β_p, $\chi_{\parallel p}$ is significantly greater in our results from the two-fluid theory than in our results from the kinetic theory. The two-fluid theory predicts a value that is approximately the observed value of $\chi_{\parallel p}$. The kinetic theory, on the other hand, underestimates the observed value by a factor between about 3 and 30 in the shown range of β_p. This observation suggests that the plasma exhibits fluid-like behavior at $k_\perp \rho_p \approx 2$.

Figure 4 shows the first perpendicular proton velocity moment $\chi_{\perp p}$ depending on β_p in both theories and our *MMS*

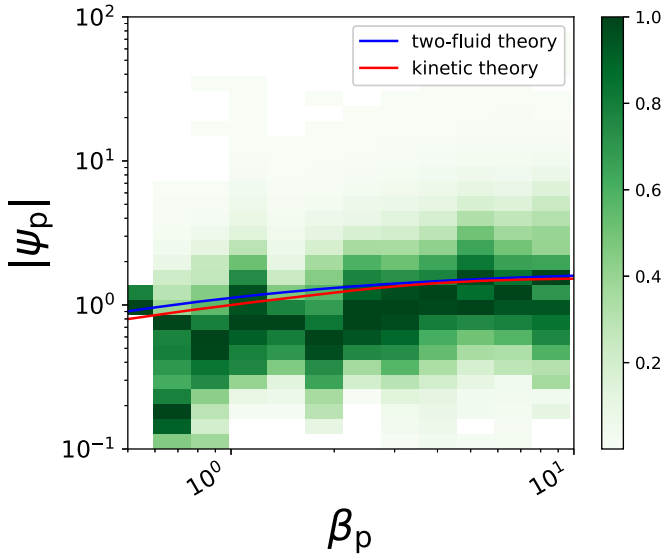

Figure 5. Ratio of ion pressure fluctuations and perpendicular magnetic-field fluctuations, ψ_p, as a function of β_p at $k_\perp \rho_p \approx 2$ with the same panel and line styles as Figure 2. The theoretical predictions for ψ_p from the two-fluid theory and kinetic theory are similar, and the observations agree with both models.

observations. The predictions from our two-fluid model are greater than the predictions from the kinetic theory by a factor of about three. The observations lie between both predictions with a small bias toward the two-fluid theory.

Figure 5 shows the second proton velocity moment ψ_p depending on β_p in both theories and our *MMS* observations. Like in Figure 2 for ξ_p, the two-fluid theory and kinetic theory predict similar values for ψ_p, and both predict the observations well.

We note that an adjustment of γ_p and γ_e within reasonable values does not lead to a significant change in our results. Moreover, an adjustment of θ_{kB} within the range of $85° \lesssim \theta_{kB} < 90°$ does not lead to a significant change in our results, confirming our assumption that the observed fluctuations are indeed consistent with highly oblique KAW turbulence.

5. Discussion and Conclusions

The behavior of KAWs departs from the behavior of Alfvén waves mainly due to two effects. The ion motion is affected by compression and introduces a polarization-drift term in the equation of motion. Furthermore, the parallel component of the electric field is non-zero and electrons move in the field-parallel direction to neutralize the ion density perturbations. We derive predictions for the proton polarization of KAWs using a collisional two-fluid theory and a collisionless kinetic theory. In the linear kinetic theory, the fluctuations are represented by fluctuations in the distribution function, δf_s, so that all moments are included and generally non-zero. Our two-fluid theory, on the other hand, assumes an adiabatic and isotropic closure for the moment hierarchy, i.e., there are no fluctuations in heat flux and the pressure tensor is isotropic. Apart from these differences, the fluid theory and the kinetic theory are equivalent. Measurements with even higher velocity-space resolution may be capable of showing the heat-flux suppression in the future.

Both theories predict similar behaviors for density and pressure fluctuations, but the parallel and perpendicular velocity fluctuations show clear differences: these fluctuations are greater in the two-fluid theory than in the kinetic theory. Due to the noise in the velocity observation, we cannot rule out the possibility that fluctuations with very small amplitude exhibit a behavior consistent with the kinetic theory. However, our comparison of fluctuations in the magnetosheath above the noise level with our theoretical predictions shows that KAW turbulence behaves fluid-like at ion scales, suggesting that some of the fluid-like behavior found by Verscharen et al. (2017) extends to the ion-scale fluctuations. We note that relaxing our assumption of temperature isotropy may improve the agreement between our theory and observations. In addition, a study based on a superposition of KAW turbulence with other modes at small scales may modify our results since our present method does not distinguish the contributions from different wave types than KAWs. A comparison with alternative approximations to the dispersion relation (Hunana et al. 2013; Sulem & Passot 2015; Told et al. 2016) may give further insight into the physics of the observed modes. However, these extensions are beyond the scope of this work.

Our finding of fluid-like behavior in KAW turbulence suggests that some yet unknown mechanism creates conditions similar to the adiabatic and isotropic closure applied in our two-fluid theory, even at small scales and under collisionless conditions. Anti-phase-mixing (Schekochihin et al. 2016) is a potential explanation for this fluid-like behavior. In the turbulent background, nonlinear interactions between fluctuations at different scales can trigger stochastic plasma echoes (Gould et al. 1967; Schekochihin et al. 2016) that may inhibit the transfer of power to higher moments of the velocity distribution. Parker et al. (2016) and Meyrand et al. (2018) find that energy transfer from large to small velocity-space scales nearly cancels due to anti-phase-mixing excited by a stochastic plasma echo. This process leads to an effective low-moment closure, even under collisionless conditions. In KAWs with larger amplitude, the nonlinear trapping of electrons may contribute to the saturation of damping and a more fluid-like behavior (Gershman et al. 2017).

Alternatively, wave–particle interactions can suppress fluctuations in higher moments of the velocity distribution. Verscharen et al. (2016) find that microinstabilities generate fluctuations that scatter protons and thus reduce the anisotropy of the pressure tensor. Wave–particle interactions may then play the role of particle–particle collisions in suppressing fluctuations in higher moments and closing the moment hierarchy at a low order.

Our finding of the fluid-like behavior of KAW turbulence at scales down to the proton inertial length supports the use of fluid models when studying large- and small-scale fluctuations. This discovery will be beneficial to astrophysical modeling since fluid computations are much faster than kinetic computations. More fundamentally, it is of great importance to determine the physics processes that lead to this fluid-like behavior of an otherwise collisionless plasma.

H.W. is supported by the China Scholarship Council for her stay at MSSL. This work is also supported by NSFC under contracts 41474147, 41674171, and 41574168, STFC Ernest Rutherford Fellowships ST/P003826/1 and ST/N003748/2, STFC Consolidated Grant ST/N000722/1, and STFC *Solar Orbiter* UK Community Support Grant ST/P005489/1. The authors appreciate the valuable conversations with Lloyd Woodham, Owen Roberts, Alexander Pitňa, Petr Hellinger,

Olga Alexandrova, and Francesco Valentini. H.W. is grateful for Chuanyi Tu's support during this work.

Appendix
Predictions for Kinetic Alfvén Turbulence in the Inner Heliosphere

In the near future, the space missions *Parker Solar Probe* and *Solar Orbiter* will carry instruments into the inner heliosphere that will provide us with unprecedented measurements of the fluctuations in both the fields and the particle distributions. Their data will allow us to study kinetic Alfvén turbulence in the solar wind using our methods for the first time.

The solar wind in the inner heliosphere exhibits a broader range of $\beta_{\rm p}$ values and typically shows $\beta_{\rm p} \approx \beta_{\rm e}$. We derive predictions for the KAW polarizations under typical solar-wind conditions with $\theta_{\rm kB} = 88°$, $T_{\parallel s} = T_{\perp s}$, $\beta_{\rm e}/\beta_{\rm p} = 1.0$, $\gamma_{\rm p} = 5/3$, and $\gamma_{\rm e} = 1$. For completeness, we add the polarizations for electrons. Our kinetic theory applies to protons and electrons likewise. In the two-fluid theory, the calculations for the electron polarizations differ from the calculations for the proton polarization. We find for electrons

$$\xi_{\rm e} = \xi_{\rm p}, \tag{29}$$

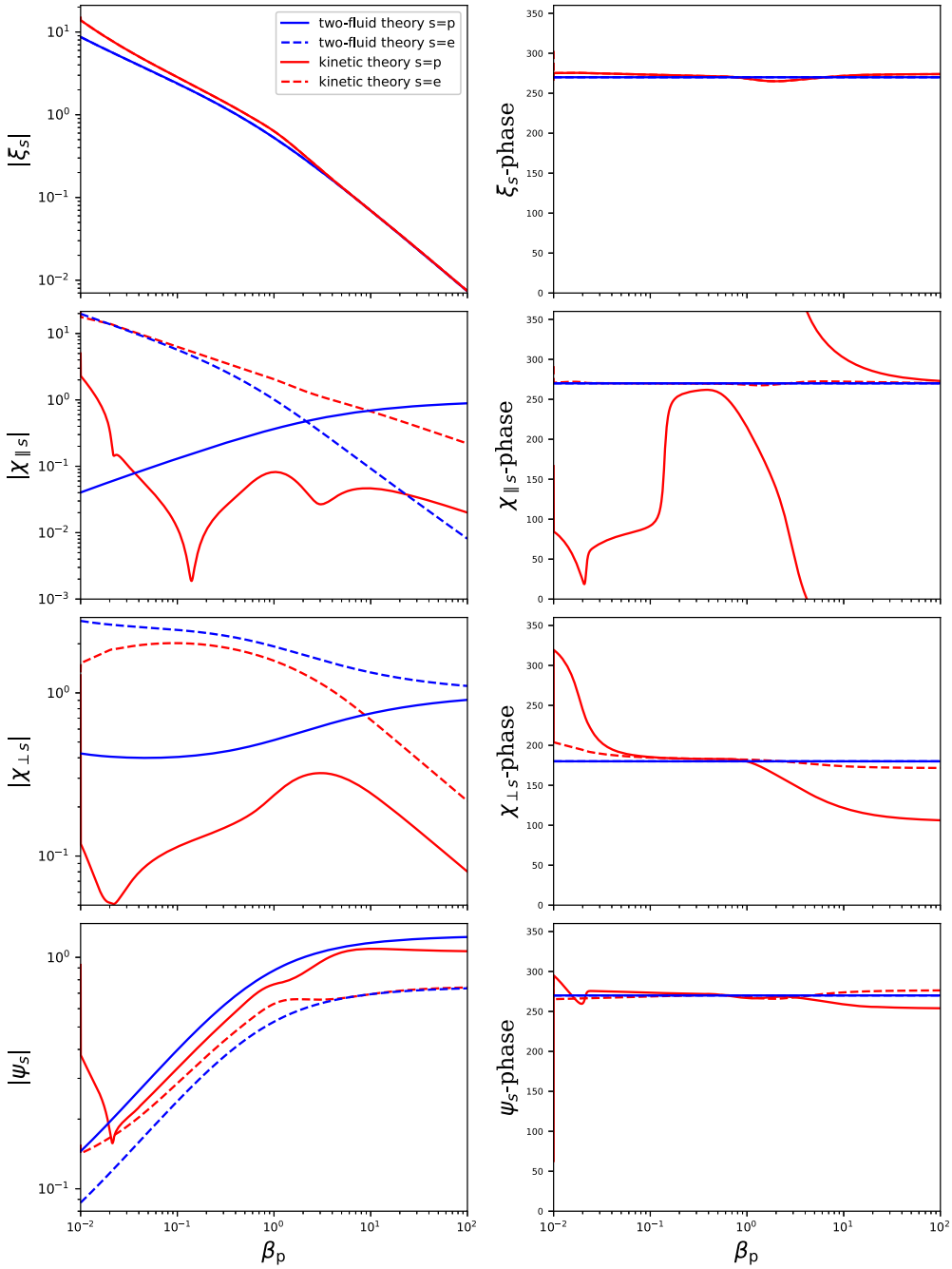

Figure 6. Predictions of KAWs as functions of $\beta_{\rm p}$ at $k_\perp \rho_{\rm p} = 2$. From top to bottom, these panels show ξ_s, $\chi_{\parallel s}$, $\chi_{\perp s}$, and ψ_s. The blue (red) lines represent the two-fluid theory (kinetic theory). The left panels show the amplitudes and the right panels show the phases. The solid (dashed) lines represent protons (electrons).

$$\chi_{\parallel e} = \left[-\frac{i\omega_{cp}}{\omega} + \frac{i\gamma_e\beta_e\omega_{cp}k_\parallel^2 v_A^2}{\omega(\gamma_e\beta_e k_\parallel^2 v_A^2 - 2\omega^2 m_e/m_p)} \right] \frac{(m_p/m_e)\ \omega\ \frac{\delta E_z}{\delta E_x}}{v_A\left(k_\parallel - k_\perp \frac{\delta E_z}{\delta E_x}\right)}, \quad (30)$$

$$\chi_{\perp e} = \left[-1 + \frac{\gamma_e\beta_e k_\perp k_\parallel v_A^2 \frac{\delta E_z}{\delta E_x}}{\gamma_e\beta_e k_\parallel^2 v_A^2 - 2\omega^2 m_e/m_p} \right] \frac{\omega}{v_A\left(k_\parallel - k_\perp \frac{\delta E_z}{\delta E_x}\right)}, \quad (31)$$

and

$$\psi_e = \gamma_e\beta_e\xi_e. \quad (32)$$

Figure 6 shows ξ_s, $\chi_{\parallel s}$, $\chi_{\perp s}$, and ψ_s at $k_\perp\rho_p = 2$ as defined in Section 2. Under solar-wind conditions, the two-fluid theory and kinetic theory predict similar ξ_s and ψ_s (in both amplitude and phase) behaviors depending on β_p. For $\chi_{\parallel s}$ and $\chi_{\perp s}$, our theoretical results show large differences in both amplitude and phase.

We expect *Parker Solar Probe* and *Solar Orbiter* to test our predictions based on large statistical data sets in the solar wind at different distances from the Sun. This future study will improve our understanding of fluctuations at ion scales and the differences between kinetic and fluid-like behavior in the solar wind.

ORCID iDs

Honghong Wu https://orcid.org/0000-0003-0424-9228
Daniel Verscharen https://orcid.org/0000-0002-0497-1096
Robert T. Wicks https://orcid.org/0000-0002-0622-5302
Jiansen He https://orcid.org/0000-0001-8179-417X

References

Belcher, J. W., & Davis, L. 1971, JGR, 76, 3534
Breuillard, H., Matteini, L., Argall, M. R., et al. 2018, ApJ, 859, 127
Burch, J. L., Moore, T. E., Torbert, R. B., & Giles, B. L. 2016, SSRv, 199, 5
Chandran, B. D. G., Quataert, E., Howes, G. G., Xia, Q., & Pongkitiwanichakul, P. 2009, ApJ, 707, 1668
Chen, C. H. K., & Boldyrev, S. 2017, ApJ, 842, 122
Chen, C. H. K., Boldyrev, S., Xia, Q., & Perez, J. C. 2013, PhRvL, 110, 225002
Chen, C. H. K., Horbury, T. S., Schekochihin, A. A., et al. 2010, PhRvL, 104, 255002
Chen, C. H. K., Mallet, A., Schekochihin, A. A., et al. 2012, ApJ, 758, 120
Chen, C. H. K., Mallet, A., Yousef, T. A., Schekochihin, A. A., & Horbury, T. S. 2011, MNRAS, 415, 3219
Gary, S. P. 1993, Theory of Space Plasma Microinstabilities (Cambridge: Cambridge Univ. Press)
Gershman, D. J., F-Viñas, A., Dorelli, J. C., et al. 2017, NatCo, 8, 14719
Gould, R. W., O'Neil, T. M., & Malmberg, J. H. 1967, PhRvL, 19, 219
He, J., Marsch, E., Tu, C., Yao, S., & Tian, H. 2011, ApJ, 731, 85
He, J., Tu, C., Marsch, E., Bourouaine, S., & Pei, Z. 2013, ApJ, 773, 72
Hollweg, J. V. 1999, JGR, 104, 14811
Horbury, T. S., Forman, M., & Oughton, S. 2008, PhRvL, 101, 175005
Hunana, P., Goldstein, M. L., Passot, T., et al. 2013, ApJ, 766, 93
Klein, K. G., Howes, G. G., & TenBarge, J. M. 2014, ApJL, 790, L20
Lucek, E. A., Constantinescu, D., Goldstein, M. L., et al. 2005, SSRv, 118, 95
Meyrand, R., Kanekar, A., Dorland, W., & Schekochihin, A. A. 2018, arXiv:1808.04284
Parker, J. T., Highcock, E. G., Schekochihin, A. A., & Dellar, P. J. 2016, PhPl, 23, 070703
Podesta, J. J. 2009, ApJ, 698, 986
Pollock, C., Moore, T., Jacques, A., et al. 2016, SSRv, 199, 331
Sahraoui, F., Goldstein, M. L., Belmont, G., Canu, P., & Rezeau, L. 2010, PhRvL, 105, 131101
Salem, C. S., Howes, G. G., Sundkvist, D., et al. 2012, ApJL, 745, L9
Schekochihin, A. A., Parker, J. T., Highcock, E. G., et al. 2016, JPlPh, 82, 905820212
Stix, T. H. 1992, Waves in Plasmas (New York: American Inst. Phys.)
Sulem, P. L., & Passot, T. 2015, JPlPh, 81, 325810103
Taylor, G. I. 1938, RSPSA, 164, 476
Told, D., Cookmeyer, J., Astfalk, P., & Jenko, F. 2016, NJPh, 18, 075001
Torrence, C., & Compo, G. P. 1998, BAMS, 79, 61
Verscharen, D., & Chandran, B. D. G. 2018, RNAAS, 2, 13
Verscharen, D., Chandran, B. D. G., Klein, K. G., & Quataert, E. 2016, ApJ, 831, 128
Verscharen, D., Chen, C. H. K., & Wicks, R. T. 2017, ApJ, 840, 106
Wicks, R. T., Horbury, T. S., Chen, C. H. K., & Schekochihin, A. A. 2010, MNRAS: Letters, 407, L31
Yan, L., He, J., Zhang, L., et al. 2016, ApJL, 816, L24